M. Nickl, S. Kaiser, A. Seitz, M. Hornung, "Performance modeling of a composite cycle engine with rotary engine", Deutscher Luft- und Raumfahrtkongress 2016, Braunschweig 2016, Document-ID 420144

PERFORMANCE MODELING OF A COMPOSITE CYCLE ENGINE WITH ROTARY ENGINE

Markus Nickl, Sascha. Kaiser, Arne. Seitz and Mirko. Hornung
Bauhaus Luftfahrt e.V., Willy-Messerschmitt-Str. 1, 82024 Taufkirchen, Germany

Abstract

Efficiency improvements of Joule-Brayton-cycle based aircraft propulsion systems became ambitious in the last decades due to technological limitations. In the present paper, the promising cycle design of Composite Cycle Engines is combined with Rotary Engine core concept and a method for rotary engine performance simulation and its integration in aircraft propulsion system synthesis is introduced. Therefore, a detailed, crank angle resolved 1D-parametric model of a rotary internal combustion engine is presented The model covers the complex geometry of rotary combustion chamber, heat losses, leakage, valve opening characteristics for rotary engine in- and outlet and crevice volumes. For the showcase of an advanced short-to-medium range aircraft application, rotary engine integration at the engine centerline is investigated. Initial results of an optimization study of rotary engine geometry and the Composite Cycle Engine performance are discussed and benchmarked against advanced Joule-Brayton cycle geared turbofan engine performance. A thrust specific fuel consumption reduction potential of 4.5% is found for the introduced concept, assuming same technology level. Due to estimated 31.2% higher power plant system weight of the Composite Cycle Engine concept compared to the geared turbofan, savings in fuel burn are supposed to be slightly smaller.

NOMENCATURE

Symbols

A	[m^2]	Area
a	[-]	Efficiency parameter of Wiebe function
BPR	[-]	Bypass ratio
d	[m]	Rotary engine rotor thickness
e	[m]	Eccentricity
FHV	[J/kg]	Fuel heating value
h	[J/kg]	specific enthalpy
k	[W/kg/m^2]	Heat transfer coefficient
l	[m]	Characteristic length
m	[kg]	Mass
m	[-]	Form factor of Wiebe function
OPR	[-]	Overall pressure ratio p_3/p_2
p	[Pa]	Pressure
R	[m]	Rotary engine rotor radius
T	[K]	Temperature
TSFC	[g/kN/s]	Thrust specific fuel consumption
V	[m^3]	Volume
v	[m/s]	velocity
VPR	[m^3]	Rotary engine rotor combustion pocket volume
w	[kg/s]	Mass flow rate
x_b	[-]	Fraction of burned fuel
α	[rad]	Crank angle
η	[-]	Efficiency
Π	[-]	Pressure ratio
ρ	[kg/m^3]	Density
σ	[N/m^2]	Mechanical stress

Subscripts

c	chamber
is	isentropic
max	maximum
min	minimum
poly	polytropic
rel	relative

Acronyms

CCE	Composite Cycle Engine
CE	Compound Engine
GTF	Geared Turbo Fan
HPC	High Pressure Compressor
ISA	International Standard Atmosphere
IPC	Intermediate Pressure Compressor
LPS	Low Pressure Spool
LPT	Low Pressure Turbine
PE	Piston Engine
RE	Rotary internal combustion Engine

Stations

0	Ambient
2	Fan inlet
21	IPC inlet
25	HPC inlet
3	RE inlet
35	Joule combustion chamber inlet
4	Turbine inlet
5	Turbine outlet
8	Core nozzle outlet
13	Bypass duct inlet
18	Bypass nozzle outlet

1. INTRODUCTION

In order to achieve aviation's long term emission reduction targets motivated by the European Commission with 'Flight-Path 2050' [1] and specified by ACARE in the Strategic Research & Innovation Agenda [2], significant improvements along the entire efficiency chain of the air transport system are required. At propulsion system level, this particularly concerns enhancements of power plant thermal or inner efficiency. In Joule-Brayton cycle machines, thermal efficiency improvements mainly result from increased Overall Pressure Ratio (OPR) and higher turbine entry temperatures (TET). For ideal cycle assumptions, i.e. ideal gas and perfect turbo component efficiencies equal to unity, thermal efficiency increases monotonically with higher OPR and TET. In reality, however, real gas properties, non-ideal components and material stress and temperature limits, which affect cooling requirements, restrict feasible efficiency improvements. Moreover, state of the art high temperature resistant materials typically increase engine bare weight, resulting in more fuel burn. Therefore, a fundamental change in aircraft engine thermodynamic cycle design is necessary.

One particularly promising option for significant efficiency enhancements beyond the Joule-Brayton cycle engines is the so-called Composite Cycle Engine (CCE) initially discussed by Kaiser et al [3,4]. This CCE concept combines the high efficiency potentials of the Seiliger cycle (isochoric-isobaric combustion), as present in piston engines, with the high specific power capability of gas turbine systems. During the forties and fifties of the last century so-called Compound Engines (CE), like the Wright R-3350 TC (1950) [5] or the Napier Nomad E.145 (1954) [6], already used a similar approach. These engines had piston systems and turbo components using the same working fluid and providing shaft power to one single output shaft. The main shaft power was delivered by the piston engines. Although the brake specific fuel consumption was almost on the level of state of the art turboprop engines the CE concept succumbed the turbo engines due to high engine weight and complexity and, even more importantly, due to limited maximum cruise speed and altitude. The CCE concept described by Kaiser et al. addresses these major drawbacks by using off-axes arranged piston systems, which only increase the work potential of the working fluid between turbo compressor and combustion chamber of the turbo engine without having mechanical connection to the turbo component shaft.

Thus, operational limitations of CEs are eliminated and additional weight and complexity compared to geared turbofan engines is reduced. Based on a CCE equipped with reciprocating piston engines and assumed year 2035 technology level, Kaiser et al. [4] identified a potential for fuel burn reduction of 36.6% compared to year 2000 turbofan technology and 18.4% against a turbofan of equal technology level.

In the present paper, the use of a Wankel-type rotary internal combustion engine (RE) in a CCE arrangement will be investigated. Compared to reciprocating piston engines, REs offer a higher power density with respect to weight and volume [7]. Furthermore, mechanical complexity and oscillations due to piston stroke are supposed to be reduced with this architecture. The Wankel-type RE is chosen for the following reasons: First, it is the functionality is proven by series produced Wankel engines such as the Mazda RENESIS and second, a reasonable level of confidence in RE performance modeling is achievable through plenty of available literature.

An initial idea for the application of a RE driving the turbo compressor within a turbofan engine concept was formulated and later on patented by J. Whurr in cooperation with Rolls-Royce in the mid-1990s [8,9]. In contrast to CCE architecture, combustion only takes place in the RE in this CE concept. Whurr performed thermodynamic cycle studies for Otto cycle core turbofan concepts by calculating the change of the thermodynamic state variables at typical stations in turbo engine architecture. RE cycle was approximated using a simplified Seiliger cycle representation. He derived rotary engine geometry and weight from required cycle data. A reduction in Specific Fuel Consumption (SFC) of about 14% compared to a Joule-Brayton cycle based turbofan was identified assuming equal technology level.

In the following, the performance modeling for a CCE architecture with RE core is discussed. A detailed, crank angle resolved model of rotary internal combustion engine and its integration in a turbo engine performance simulation framework is presented. Finally, as a showcase, initial results of cycle studies, varying RE geometry, TET and OPR are illustrated for a generic, advanced short-to-medium range narrow body aircraft application.

2. ADVANCED CYCLE DESIGN OF CCE

To increase thermal efficiency beyond Joule-Brayton limitations in CCEs a second cycle with independent compression, combustion and power extraction (expansion) is added. In the current study, a Seiliger cycle with closed volume compression and expansion and partial constant volume combustion as can be technically achieved with a Wankel-type RE is used. Especially for high pressure application,

compression efficiency of piston engines is far above that of turbo engines. Furthermore, the additional pressure rise during isochoric combustion reduces the power demand of the engine for compression.
As depicted in FIG 1 the Seiliger cycle is embedded in the Joule-Brayton cycle, starting at the end of Joule cycle compression. It is instationary and composed of closed volume compression and isochoric-isobaric combustion and expansion. Heat losses from RE, which typically have to be dissipated, e.g. in automotive applications, can be rejected to the core engine fluid in the CCE concept. Thus, higher heat losses from RE compared to reciprocating engines reduce the heat addition in the Joule combustion chamber for a given TET.

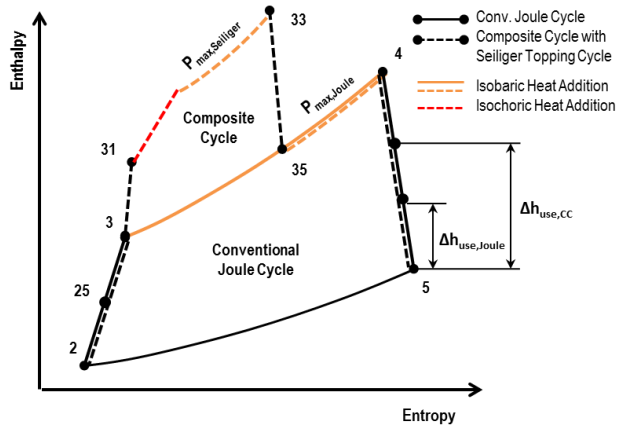

FIG 1. Enthalpy of entropy -diagram of the Composite Cycle and conventional Joule-Brayton Cycle

The resulting CCE cycle separates into polytropic compression with turbo components (1→3), closed volume compression in the RE (RE, 3→31), isochoric-isobaric combustion (RE, 31→33), closed volume expansion (RE, 33→35), isobaric combustion in the Joule combustion chamber (35→4) and polytropic expansion in the turbine (4→5).

3. DESCRIPTION OF CONCEPT ARCHITECTURE

The combination of discontinuous Seiliger cycle of the RE with continuous Joule-Brayton turbo engine cycle implies some additional requirements for engine architecture. For instance, discontinuity in the mass flow rate at the RE inlet generate pressure fluctuations upstream, which might reduce turbo compressor efficiency and affect surge margin. Therefore buffer volumes are necessary to reduce these pressure fluctuations to an acceptable level.

The CCE with RE core investigated in the current study is generally designed as high bypass ratio geared turbofan (GTF), which means, that the fan is driven by a fast running turbine and the fan rotational speed is reduced by a gear box. After the fan rotor, mass flow is separated core and bypass flow. The core mass flow enters the Intermediate Pressure Compressor (IPC) and the High Pressure Compressor (HPC) compressor. The IPC is directly driven by the turbine, whereas the HPC is powered by the RE. After the HPC a buffer volume is installed to reduce pressure fluctuations from instationary RE operational behavior. The mass flow coming from the HPC outlet is buffered in this volume and from there distributed to the single disks of the RE. In addition, air is taken from the HPC outlet mass flow rate for RE cooling and later on mixed with RE outlet mass flow.
For RE, an arrangement coaxial to the main centerline of the turbo engine is investigated. The most beneficial number of installed rotor disks will be determined by a RE geometry study in section 5.2. As illustrated in FIG 2 the diameter of the RE disks, depicted as rectangles, subdivided in crank shaft (green), rotor (grey) and chamber volume (flame colors), exceed the radial dimensions of the HPC. Nevertheless, maximum relative velocity between RE casing and the rotor apex is limited to significantly lower values than HPC tip speed, restricting the maximum rotational speed of the RE to relatively low numbers of revolutions. Therefore, an additional gearbox between HPC and RE is installed to realize reasonable HPC tip speeds. After the RE a second buffer volume collects the mass flows from the RE disks. In the following Joule combustion chamber second combustion takes place. Finally, the hot gas expands into the turbine and the extracted power is delivered to the fan via the Low Pressure Spool (LPS). For turbine-fan connection, the LPS has to cross the RE at the centerline of the engine.
The required thrust is mainly provided by the mass flows leaving the engine through an unmixed bypass nozzle. The residual thrust coming from the core nozzle is also considered. Between all components ducting is inserted with reasonable losses.

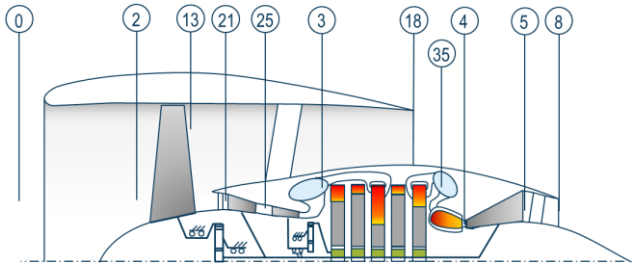

FIG 2. Basic conceptual sketch of a CCE with coaxial rotary internal combustion engine

4. DESIGN AND ANALYSIS METHODS

During turbo engine and RE performance simulation fluid properties are calculated over a wide range of temperatures and pressures causing large errors when ideal gas properties are used [4]. For pressure variations the change of fluid properties are comparably small. Therefore half-ideal gas properties, which reflect temperature dependency only, are used in the current study based on polynomials representation from NASA's Chemical Equilibrium with Applications database [10].
The applied methods for turbo engine performance simulation calculate the change of thermodynamic state variables at the stations shown in FIG 2. Mechanical and aerodynamic restrictions and requirements especially of the turbo compressors, turbines, ducts and nozzles are considered.
A MATLAB® based, modular in-house framework is used for turbo engine performance simulation, which was validated with negligible deviation against the commercial software GasTurb® for design point and off-design calculation.

4.1. Rotary Engine cycle modeling

The complex, instationary behavior and implications of design parameter variations of REs cannot be sufficiently reproduced by the simple thermodynamic Seiliger cycle representation. Especially differences in scavenging behavior, heat losses and leakage and their effects on RE performance need to be represented in dependency of RE geometry changes. Therefore, a 1D time resolved modeling approach for RE geometry and thermodynamics is used. For given geometry, fluid inlet conditions, rotational speed and defined fuel-air-ratio, the model delivers all relevant performance parameters of the RE at the outlet, including mass flows, power release, heat transfers and outlet conditions.

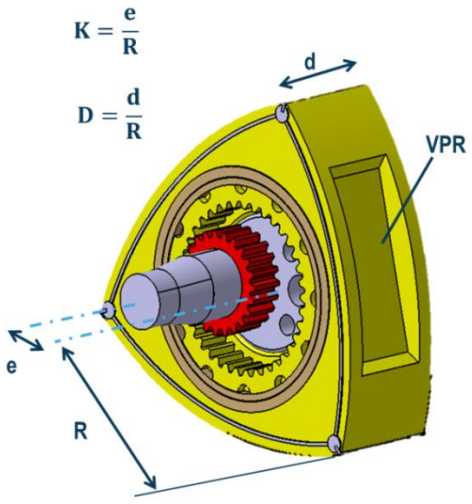

FIG 3. Basic sketch of a rotary engine rotor (yellow) with power shaft (grey) and key geometry parameter (based on [11])

RE geometry is mainly determined by rotor radius R, eccentricity e rotor thickness d and rotor combustion pocket volume VPR as depicted in FIG 3. The inner (radial) casing shape results from the curve drawn by the rotor apex during rotation. The chamber volume at each crank angle position α is given by

$$(1)\quad V_c = V_{min} + \frac{3\sqrt{3}}{2} eRb\left\{1-\sin\left(\frac{2}{3}\alpha+\frac{\pi}{6}\right)\right\} + VPR,$$

$$(2)\quad V_{min} = \left\{\frac{e^2}{3} + 2eR\cos\varphi_{max} + \left(\frac{2}{9}R^2+4e^2\right)\varphi_{max} - \frac{3\sqrt{3}}{2}eR\right\} d$$

with $\sin(\varphi_{max}) = 3e/R$.

Radial and lateral casing surface areas, which are relevant for heat transfer, are determined by

$$(3)\quad A_{rad} = d\int_{\alpha}^{\alpha+2\pi}\frac{1}{3}\sqrt{9e^2+R^2+6eR\cos\left(\frac{2}{3}x+\frac{\pi}{2}\right)}\,dx$$

$$(4)\quad A_{side} = \frac{V_c - VPR}{d}.$$

For heat transfer from the fluid in the chamber to the rotor, surface enlargement due to rotor pocket is neglected.

In- and outlet valves of the RE are assumed to be located at the lateral chamber walls and are set to maximum geometric feasible area. It was found that maximum valve areas lead to best engine performance due to best scavenging behavior. When RE geometry is modified, these areas are assumed to scale proportionally to rotor radius R and eccentricity e. Additionally, valve area opening and closing characteristics are assumed sinusoidally. Only one third of the time between valve opening and closing maximum valve area is available. Valve opening and closing timings are set to performance optimized values for engine geometry given in [12] and are kept constant for all other geometry and performance parameter variations.

Variable	Unit	Value
Intake Valve Opening	[deg]	770
Intake Valve Closing	[deg]	0
Outlet Valve Opening	[deg]	450
Outlet Valve Closing	[deg]	780
Start of Combustion	[deg]	200
End of Combustion	[deg]	290

TAB 1. Rotary engine port and combustion timings

In REs, leakage from one chamber to the previous and the following chamber around the apex and side seals leads to significant decrease of achievable output power. For the current model these two leakage mass flows are determined by pressure difference between the chambers and an equivalent leakage area, which was calibrated to match

validation data given in [12]. Leakage area is assumed to scale proportionally to rotor radius R and rotor thickness d for RE geometry variation.

By evaluating the heat transfers at the inner and outer chamber walls the heat losses during RE cycle are computed. Therefore, a surrounding fluid flow with Mach number 0.1 and inlet fluid conditions are assumed at the outer wall of the engine. An associated heat transfer coefficient k is derived from Nusselt number correlation for fluid flow over a flat plate, using a characteristic length $l \sim (R + e)$. At the inner chamber wall, heat transfer coefficient is also calculated from a Nusselt number correlation which is valid for forced convective heat transfer conditions. Here, characteristic length is given by rotor thickness d and characteristic velocity is correlated with rotor apex velocity. During combustion, higher heat transfer rates are assumed, following the approach published by Woschni [13]. The heat transfer model is calibrated to the data published in [12]. The temperature of the rotor is assumed to be uniform and constant and is derived from the energy balance across the rotor surfaces oriented to the three chamber volumes.

The time resolved heat release of internal combustion process in REs is modeled by the Wiebe function [14]

$$x_b = 1 - e^{-a\left\{\frac{\alpha-\alpha_0}{\Delta\alpha_b}\right\}^{m+1}}, \quad (5)$$

The fraction of burned fuel x_b is described by α, the current crank angle position, α_0 the position of combustion start and $\Delta\alpha_b$ the range of crank angels in which combustion takes place. With the Wiebe parameters *a* and *m* the heat release can be modified to the characteristics of individual engines. For the current paper, *a* = 5 and *m* = 1.5 as given in [9] were chosen. Compared to typical reciprocal piston engines ($\Delta\alpha_b \approx 45°$) heat release in REs occurs over a wider range of crank angle positions ($\Delta\alpha_b \approx 80°$) [15]. In the current study, combustion start an duration is also chosen according to [12].

By iteratively solving the mass and energy balance between RE in- an outlet, mass flow averaged thermodynamic state variables at the exhaust and other important performance parameters like power output, fuel flow, peak pressure wall temperatures and resulting heat losses are determined.

4.2. Weight estimation and component scaling

As piston engine systems have typically a lower power-to-weight ratio than turbo engines, system weight of the introduced engine has to be considered for propulsion system assessment. Therefore, a weight estimation model is according to [16] is implemented. RE casing weight is calculated with

$$m_{casing} = \frac{\pi R^2 \cdot (1+(e/R))^2 \cdot p_{max}}{\sigma/\rho} \cdot \{2/3 \cdot nR + R(n+1)(1+e/R)\} \quad (6)$$

from engine geometry data (eccentricity *e*, rotor radius *R* and number of rotors n resulting from cycle calculation), peak cycle pressure p_{max}, and material properties (density ρ and tensile strength σ). To consider cooling fins, casing weight is corrected by the factor 1.5 ($m_{cooling\_fin} = 0.5 \cdot m_{casing}$). The rotor weight is derived from the rotor volume and its material density, assuming half of the rotor volume being hollow:

$$m_{rotor} = n \cdot 0.5 \cdot V_{rotor} \cdot \rho_{rotor} \quad (7)$$

By summing the weights of casing, cooling fins and rotors bare engine weight is determined

$$m_{bare} = m_{casing} + m_{cooling\ fin} + m_{rotor}. \quad (8)$$

Finally, bare engine weight is increased by the factor of 1.18 to account for bearings, mountings, shafts and other structural elements for engine integration.

For turbo component weights a delta assessment to reference geared turbo fan components presented in [17] is employed. To this end, turbo engine components are divided into two categories, one including components which are connected to the propulsive device (bypass duct, fan, nacelle, etc.) and another which contains the core engine related components. First category components are assumed to scale with the fan diameter, whereas the core engine related component weights are estimated to scale with the corrected core mass flow.
Beside weights, component efficiencies are also correlated to component size. Especially for compressor efficiencies i.e. relative gap size has important influence on component efficiency and has to be considered, if same technology level is assumed. Therefore turbo component efficiencies are set for the advanced GTF reference and are scaled for CCE for RE again using the mean corrected mass flow of the component.

4.3. Rotary Engine Model Verification

The previously described model for RE performance calculation is validated with the data presented in [12]. Therefore, an engine model is set up, using identical parameters for geometry, port and combustion timing, valve areas, revolution and fluid inlet conditions.
As can be seen from TAB 2 the calculated integral performance values for the RE match the reference data within a deviation less than 2.5%. For initial analysis of the potential of a CCE with RE core this

accuracy is sufficient.

Variable	Unit	Ref.	RE	Delta
Power	[kW]	22.8	22.8	+/-0.0
Heat Loss	[kW]	16.3	16.0	-2.1
Fuel Flow	[g/s]	0.58	0.57	-2.3%
Thermal Efficiency	[%]	29.7	30.1	+1.3%
Volumetric Efficiency	[%]	75.9	76.9	+1.3%
Max. Pressure	[bar]	41.2	41.6	+1.1%

TAB 2. Integral verification results of rotary engine performance model, reference data from [12]

Main focus of RE modeling was to generate a satisfactorily representation of the instationary process which takes place in the chambers of the RE during crank shaft rotation. In FIG 4 (a) to (c) the crank angle resolved results for pressure, temperature and heat losses for one RE chamber are depicted. While the absolute level of heat losses is calibrated to match the reference data (c), the modeling of the heat transfer coefficients and the

a)

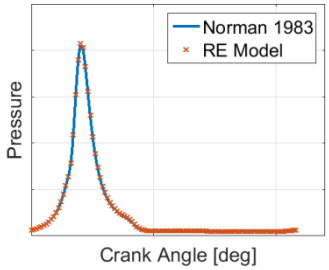

b)

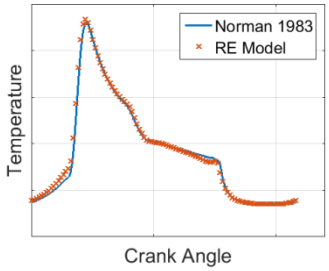

c)

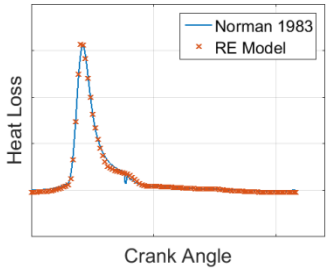

FIG 4. Crank Angle resolved calculation results of RE model for a) chamber pressure b) chamber temperature and c) heat losses validated with data given in [12].

corresponding areas, which affect the general shape, is proven by the validation data. Pressure (a) and temperature (b) characteristics are independent results of the RE modeling and fit the reference data with very good agreement. For all three parameters sufficient representations of the general behavior are achieved. Only small deviations are observed e.g. for temperatures quite before the combustion starts and temperature rises. This is resulting from the assumption of uniform RE casing temperature leading to an overestimation of the wall temperature during the chamber charging interval. A small amount of heat is transferred into the chamber volume, cumulating to the depicted temperature difference, although no significant deviation in heat transfer is detected

4.4. Integration in Aircraft Propulsion System Synthesis

For evaluation of RE performance in a CCE architecture the previously described performance model of RE is integrated into the BHL in-house Aircraft Propulsion System Syntheses (APSS) framework. In APSS, a component based, modular turbo engine architecture representation is used for power plant performance calculation. During cycle calculation iterations common sizing and design heuristics reported in [17,18] are applied. Following the flow path through the engine, changes in thermodynamic state variables are computed. As the RE engine drives the HPC, the required shaft power from RE known. With fluid input conditions according to HPC outlet and a technologically limited maximum peak pressure in RE cycle, a RE geometry, which is able to fulfill the performance requirements, is derived. The gearbox between HPC and RE moderates the resulting differences in rotation speed of HPC and RE. Finally, Top Of Climb (TOC) conditions and requirements are used for engine and flow path sizing assuming typical turbo component axial Mach numbers and hub-to-tip ratios as published in [19].

4.5. Evaluation Metrics

As indicators for power plant system improvement typical performance metrics on engine level are used. Most importantly, the Thrust Specific Fuel Consumption

$$(10) \quad TSFC = \frac{w_{fuel}}{F_N}$$

is determined by the division of the fuel flow w_{fuel} and the net thrust F_N.
Furthermore, core efficiency

$$(11) \quad \eta_{core} = \frac{P_{core}}{P_{supply}} = \frac{w_4(\Delta h_{is} - 0.5v_0^2)}{w_{fuel} \cdot FHV}$$

is evaluated. For the deviation of fuel burn and CO_2

emission reduction potentials of the propulsion system, power plant system weight also has to be considered. With TSFC and PPS weight the impact on fuel burn can be modeled for a reference aircraft platform, which is not part of this investigation.

5. RESULTS

In the current paper the introduced integrated CCE-RE model is adapted to the showcase of the propulsion system of a generic advanced short-to-medium range narrow body aircraft platform with entry into service in Y2035+. The required maximum net thrust at TOC settings (Altitude 10668m, ISA+10, Mach number 0.78) is estimated to be approximately 20% lower than today. This reduced thrust requirement is an outcome of expected airframe efficiency improvements and assumed aircraft weight savings due to reduced structural weight and less fuel weight due to fuel burn reduction resulting from PPS efficiency enhancement.

5.1. General cycle settings

General cycle settings (including e.g. reference component efficiencies, pressure losses) as listed in TAB 3 are applied to a reference GTF and CCE with RE core. The values are assumed for an advanced Y2035+ technology level. Fan diameter is fixed for best engine core cycle comparability. Additionally, CCE-RE specific parameters, like peak cycle pressure, mean rotor apex velocity and rotor depth ratio D = d/R are illustrated in TAB 2. These parameters are estimated to reflect best practice advanced technology level. Peak cycle pressure at TOC is limited to 120bar, assuming this would result in the maximum allowable peak pressure of 300 bar for take-off settings. In case of CCE, HPC pressure ratio is fixed to Π_{HPC} = 6 and IPC pressure ration is adapted to reach the given OPR. Otherwise, increasing Π_{HPC} would lead to higher power request from RE, which has to be generated from reduced core mass flow. In combination with limited peak pressure during RE cycle due to maximum material stress limitations a setting with increasing Π_{HPC} is not feasible.

Variable	Unit	Value
General		
Polytr. Fan Efficiency	[-]	0.94
Polytr. IPC Efficiency	[-]	0.92
Polytr. HPC Efficiency	[-]	0.91
Polytr. HPT Efficiency	[-]	0.92
Polytr. LPT Efficiency	[-]	0.94
Duct Pressure Ratios	[-]	0.99
Combustion Chamber pressure ratio	[-]	0.97
Fuel Heating Value	[MJ/kg]	42.8
Fan Diameter	[m]	2.20
Gearbox Efficiency	[-]	0.99
Nozzle coefficients	[-]	0.99
CCE with RE		
Peak Cycle Pressure	MPa	12
Mean Rotor Apex Velocity	[m/s]	39
D-Factor d/R	[-]	2/3
HPC Pressure Ratio	[-]	6

TAB 3. General cycle settings and RE specific parameters

With these settings, two parameters studies are performed. On the one hand, most efficient general RE geometry will be identified in terms of e/R ratio (range: 0.1… 186) and the number of rotors for RE centerline arrangement (range: 3…10). Changes in RE geometric compression ratio due to eccentricity ratio variation are compensated by rotor pocket volume adaptation to stay within the peak cycle pressure limitation. For RE geometry study T_4 = 1400K and OPR = 20 is chosen. On the other hand, as main study parameters to identify the optimum cycle design, turbine entry temperature T_4 (range: 1300K…2000K) and Overall Pressure Ratio (OPR = p_3/p_2, range 10…30) are chosen.
Finally, the performance of the most beneficial CCE-RE design is compared to an advanced GTF reference. For GTF performance calculation T4 = 1750 and OPR = 60 are chosen.

5.2. Rotary Engine Design

In FIG 5 the influence of RE eccentricity ratio e/R on TSFC and RE system weight is depicted. With increasing e/R ratio TSFC and RE system weight reduce. Therefore, high e/R ratios are desirable. The reduction in RE system weight results from increasing displacement volume with rising eccentricity ratio for fixed rotor radius R. In consequence, the given core mass flow from the HPC can be handled by a smaller, lighter RE. TSFC improvement results from changes in RE casing and

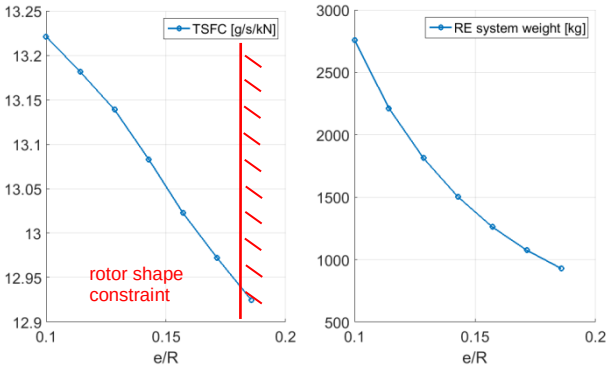

FIG 5. Thrust specific fuel consumption (left) and RE system weight (right) for various e/R-ratios

rotor shape for different eccentricity ratios. For higher e/R ratios, feasible in- and outlet areas at the lateral walls of RE increase, leading to improved scavenging and thus, to more efficient REs. Additionally, enhanced eccentricity ratios ease the integration of the LPS into the RE architecture, because increasing crank shaft diameters are viable.

In a second step, the influence of RE rotor disk sizing on TSFC and RE system weight was investigated by variation of the number of RE rotors. The results are shown in FIG 6. While TSFC is up to 4.8% (3 rotor disks) lower for fewer, larger rotors, weight increases by up to 73.7% (3 rotors), in relation to CCE-RE with 10 rotor disks. TSFC improvement for fewer rotors results from improved surface to volume ratio of RE chamber, leading to reduced heat losses. Furthermore, leakage relative to chamber volume is also lower, leading to improvements in RE power extraction. The monotonously decreasing TSFC for increased RE size and especially the rising gradient of the reduction in case of 3-4 rotors indicates, that area scaling for in- and outlet valves or the equivalent leakage area seems to be inappropriate for these cases and has to be refined.
Weight reduction for increasing RE rotor numbers is induced by RE radial size reduction. The boundary condition of constant mean rotor apex velocity supports the effect of RE diameter decrease. The loss in displacement volume per revolution for higher number of rotors is compensated by higher allowable rotational speeds due to shorter circumference of the RE.

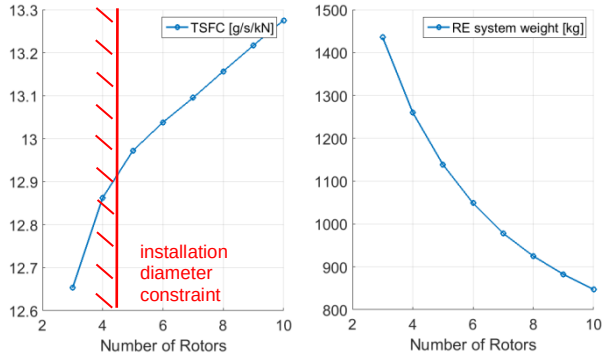

FIG 6. Thrust specific fuel consumption (left) and RE system weight (right) for different numbers of RE rotors

Based on the described RE geometry design studies design criteria for eccentricity ratio and the number of rotor disks are identified. First, eccentricity ratio has to be chosen maximal, leading to TSFC and RE system weight reduction. But geometrical limitations of the rotor have to be considered. For e/R>0.2 the rotor shape oriented to the chamber volume turns from convex to concave even without a rotor pocket volume for combustion. Concave rotor surfaces at the combustion chamber would lead to less shaft power, because temporarily for some rotor surface areas torque contrary to shaft rotation would be induced during expansion. Therefore, eccentricity ratio is chosen at 0.171, to be account for this effect.
For the ideal number of RE rotors, TSFC reduction has to be traded with the increase in weight. Additionally, RE diameter is limited by the core cowling diameter. From approximated RE diameters and an analyses of typical core cowling diameters of state of the art turbo engines of the investigated thrust level it was derived, that for less than 5 rotors, RE diameter would exceed typical core cowling shape. Since a TSFC improvement of approximately 0.5% from 6 to 5 rotors is expected to overbalance the weight penalty of approx. 110kg a RE rotor disk number of 5 is chosen for further investigations.

5.3. Cycle Design

With the RE geometry parameters determined in section 5.2 and parameter ranges defined in section 5.1, a Joule-Brayton cycle optimization study is performed.
In FIG 7, the impact of T_4 and OPR on thrust specific fuel consumption and engine core efficiency is depicted. An optimum for both parameters can be found at OPR = 23.3 and T_4 = 1300K. Due to fixed fan diameter, core efficiency and TSFC exhibit nearly identical characteristics during T_4-OPR variation. Low T_4 temperatures are beneficial in terms of TSFC, because less fuel is combusted in the inefficient Joule combustion chamber and a higher fraction of more efficient closed volume combustion in the RE is reached. Furthermore, less turbine cooling air is required for lower turbine entry temperatures, resulting in higher core efficiencies. TSFC and η_{core} rises monotonously with rising T_4 at constant OPR.
Due to the limited peak pressure in RE cycle, TSFC optimum is not found for maximum OPR. Increasing OPR leads on the one hand to higher charged, more efficient rotary engines and to more efficient combustion in the Joule combustion chamber (resulting from diverging isobars in T-s diagram). On

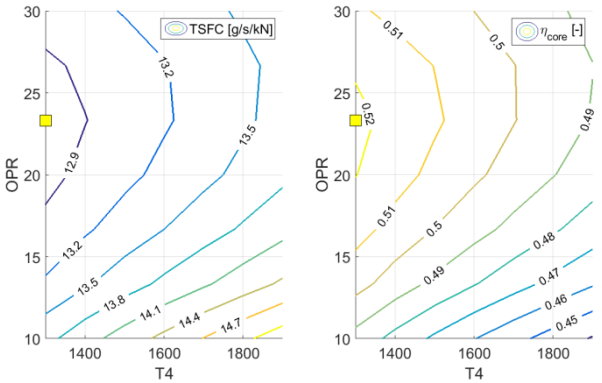

FIG 7. Thrust specific fuel consumption (left) and core efficiency (right) for T4-OPR study

the other hand, this effect is superimposed by decreasing compression ratio and size reduction of the RE, which both decrease RE efficiency.

Beside TSFC and η_{core}, bypass ratio and power plant system weight is evaluated. The results are shown in FIG 8. While BPR rises monotonously with T_4 only a second order dependency of BPR on OPR is detected. With increasing T_4 a gain of specific work potential in the turbine is achieved. In consequence, core mass flow is reduced and with constant fan diameter, BPR rises. The effect of enhanced core efficiency for low T_4, which would allow for higher BPR, is completely covered by the gain of specific work potential at the turbine inlet.
Power plant system weight sensitivity is dominated by the influences of RE installation weight and turbo component scaling, which are connected to the corrected core mass flow. Due to constant fan diameter, weights correlating with the propulsive device (nacelle, fan blades, etc.) are constant for both concepts. As previously explained, core mass flow and core size are decreasing with increasing T_4. Therefore, PPS weight shows a similar behavior. Moreover, a sensitivity to OPR is observed, mainly resulting from reducing RE size and system weight with increasing OPR.

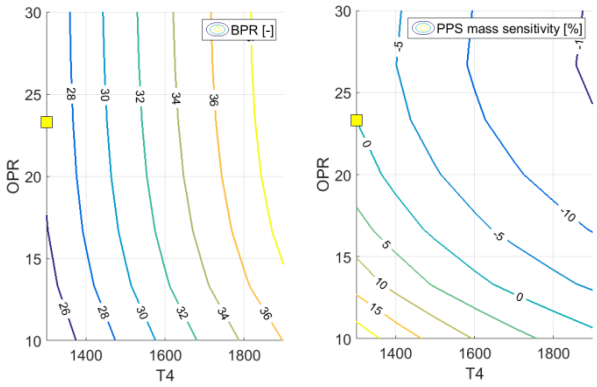

FIG 8. Bypass Ratio (left) and Power Plant System mass sensitivity (right) for T_4-OPR study

In further investigations trade factor for fuel burn on mission level for the application case will be determined to identify the optimum T_4 by trading TSFC improvement (low T_4) with PPS weight decrease (high T_4). In a first step, according to best practice experience, optimum T_4 is set to 1300K. For OPR an optimum of OPR = 23.3 is identified.

5.4. Performance comparison of CCE-RE and advanced GTF

In TAB 4 a comparison of advanced reference GTF performance data at TOC conditions with the optimized CCE-RE cycle data is illustrated. For CCE-RE concept, a 400K lower T_4 is identified to be TSFC optimal. The required turbine cooling air at take-off is therefore estimated to be 68% lower than for the advanced GTF. A TSFC reduction potential of 4.5% compared to advanced GTF reference is obtained, while PPS weight increases 31.2%. The low OPR of 23.3 helps to minimize weight penalty of CCE-RE concept due to fewer turbo engine stages. A fraction of 82.6% of total combusted fuel is burned in the RE for the CCE concept. Due to higher core specific work, BPR increases to 26.4 compared to GTF reference (BPR_{GTF} = 19.1). In TAB 5. the resulting RE geometry parameter are listed.

Variable	Unit	GTF	CCE-RE
T_4	[K]	1750	1300
OPR	[-]	60.0	23.3
TSFC	[g/KN/s]	13.3	12.7
$\Delta\eta_{core}$	[%]	Ref	+4.7
m_{PPS}	[%]	Ref	+31.2
Π_{Fan}	[-]	1.33	1.33
BPR	[-]	19.1	26.4
$w_{cool,rel}$	[%]	23.8	7.6
$w_{fuel,joule,rel}$	[%]	100	17.4
w_{Rstd25}	[kg/s]	11.6	8.45

TAB 4. Comparison of selected performance data for GTF and CCE-RE

Variable	Unit	Value
Rotor Radius	[m]	0.331
Eccentricity	[m]	0.057
Rotor Depth	[m]	0.220
Rotary Engine System Weight	[kg]	1240
Approx. Diameter	[m]	~0.90
Approx. Axial Length	[m]	~1.40

TAB 5. Rotary engine geometry parameter for optimum cycle parameter

6. CONCLUSION

The introduced analyses methods for 1D rotary engine cycle performance calculation and integration into turbo engine performance syntheses allow a detailed evaluation of the thrust specific fuel consumption reduction potential of Composite Cycle Engines with rotary internal combustion engine core. The models incorporate rotary engine's geometry specific scaling behavior of main performance parameter as well as detailed representations of turbo engine components and their scaling characteristics. For the chosen Composite Cycle Engine architecture with three compressors and the high pressure compressor powered by a rotary engine, which is integrated at the engine centerline, benefits and drawbacks are identified. On the one hand, the Composite Cycle Engines with coaxial rotary engine core integration provides a thrust

specific fuel consumption reduction potential of 4.5% beyond an advanced geared turbofan with Joule-Bryton cycle, while assuming Y2035+ technology level for both concepts. The optimum cycle parameters are found for significantly lower burner exit temperature (T_4 = 1300K) and Overall Pressure Ratio (OPR = 23.3), compared to advanced geared turbofan reference (T_4 = 1700, OPR = 60). On the other hand, huge differences in rotational speeds and limited rotary engine apex velocity affect the requirement of an additional gearbox between high pressure compressor and rotary engine, increasing the complexity of the investigated engine arrangement. Due to restrictions resulting from the geometric installation space inside the core cowling and rotational speed limitations of the rotary engine, the theoretical thrust specific fuel consumption saving and integration potential of the Composite Cycle Engine with centerline rotary engine concept was not exploited in the initial study presented in this paper. In further investigations, these limitations have to be addressed by the use of other engine architectures, which allow e.g. the integration of the rotary engine with larger diameters and/or lower rotating speeds.

REFERENCES

[1] European Commission, “Flight-Path 2050: Europe’s Vision for Aviation”, Publications Office of the European Union, Luxembourg, 2011.

[2] ACARE, “Strategic Research & Innovation Agenda - Volume 1”, 2012.

[3] Kaiser et al., “A Composite Cycle Engine Concept with Hecto-Pressure Ratio”, 51st AIAA/SAE/ASEE Joint Propulsion Conference, Orlando, FL, 2015.

[4] Kaiser et al., “Unified Thermodynamic Evaluation of Radical Aero Engine Cycles”, ASME Turbo Expo, Seoul, 2016.

[5] „Facts about the Wright Turbo Compound“, Curtiss-Wright Corporation, Wright Aeronautical Devision, Wood-Ridge, NJ, 1956.

[6] Flight Global, “Napier Nomad – An Engine of Outstanding Efficiency”, Flight Global, 04.1954, pp 543-551.

[7] “Mazda Wankel Rotary Engines for Aircraft”, ULR: http://www.rotaryeng.net [last access 05.September 2016].

[8] Whurr, “Otto Cycle Core Turbofan Concepts” MSc Thesis Canfield University, 1995.

[9] Whurr, “Aircraft Compound Cycle Propulsion Engine” US Patent Nr. 5692372, 1997.

[10] Gordon, S., and Mcbride, B.J., “Computer Program for Calculation of Complex Chemical Equilibrium Compositions and Applications”, Cleveland, Ohio, 1994.

[11] https://d2t1xqejof9utc.cloudfront.net/screenshots/pics/c2ffad7a83bcf5cb5fe3d73180aa88fa/large.bmp [last access 05.September 2016].

[12] Norman, “A Performance Model of a Spark Ignition Wankel Engine Including the Effects of Crevice Volumes, Gas Leakage and Heat Transfer” MIT, ME M.Sc.-Theses, 1983.

[13] Woschni, "A Universally Applicable Equation for the Instantaneous Heat Transfer Coefficient in the Internal Combustion Engine", SAE Transactions, Vol. 76, paper 670931, 1968.

[14] Wiebe, I., “Brennverlauf und Kreisprozess von Verbrennungsmotoren”, VEB Verlag Technik, Berlin, 1970.

[15] Zima, S., “Ungewöhnliche Motoren”, Vogel Business Media, Würzburg, 2010.

[16] Civinskas, K.C., Kraft, G.A. “Preliminary Evaluation of a Turbine/Rotary Combustion Compound Engine for a Subsinic Trasport Aircraft”, NASA Technical Memorandum TM X-71906, 1976.

[17] Seitz, A., „Advanced Methods for Propulsion System Integration in Aircraft Conceptual Design“, Dissertation Technische Universität München, 2012.

[18] Grieb, H., “Projektierung von Turboflugtriebwerken”, Birkhäuser Verlag, Basel-Boston-Berlin, 2004.

[19] Schaber, R. “Numerische Auslegung und Simulation von Gasturbinen”, Dissertation Technische Universität München, 2000.